Harnessing a Novel P450 Fatty Acid Decarboxylase from *Macrococcus caseolyticus* for Microbial Biosynthesis of Odd Chain Terminal Alkenes

Jong-Won Lee[1,2,§], Narayan P. Niraula[3,§,#], and Cong T. Trinh[1,2,3,*]

[1]Bredesen Center for Interdisciplinary Research and Graduate Education, University of Tennessee, Knoxville, TN, USA

[2]Center for Bioenergy Innovation, Oak Ridge National Laboratory, Oak Ridge, TN, USA

[3]Department of Chemical and Biomolecular Engineering, University of Tennessee, Knoxville, TN, USA

[§]Equal contributions

[*]Corresponding author. Email: ctrinh@utk.edu

[#]Current address: Pfizer Inc., Kalamazoo, MI

Running title: Harnessing $OleT_{MC}$ for terminal alkene synthesis in *E. coli*

ABSTRACT

Alkenes are industrially important platform chemicals with broad applications. In this study, we report a microbial conversion route for direct biosynthesis of medium and long chain terminal alkenes from fermentable sugars by harnessing a novel P450 fatty acid (FA) decarboxylase from *Macrococcus caseolyticus* ($OleT_{MC}$). We first characterized $OleT_{MC}$ and demonstrated its *in vitro* H_2O_2-independent activities towards linear and saturated C10:0-C18:0 FAs, with the highest activity for C16:0 and C18:0 FAs. Combining protein homology modeling, *in silico* residue mutation analysis, and docking simulation with direct experimental evidence, we elucidated the underlying mechanism for governing the observed substrate preference of $OleT_{MC}$, which depends on the size of FA binding pocket, not the catalytic site. Next, we engineered the terminal alkene biosynthesis pathway, consisting of an engineered *E. coli* thioesterase (TesA*) and $OleT_{MC}$, and introduced this pathway into *E. coli* for direct terminal alkene biosynthesis from glucose. The recombinant strain *E. coli* EcNN101 produced a total of 17.78 ± 0.63 mg/L odd-chain terminal alkenes, comprising of 0.9% ± 0.5% C11 alkene, 12.7% ± 2.2% C13 alkene, 82.7% ± 1.7% C15 alkene, and 3.7% ± 0.8% C17 alkene, and a yield of 0.87 ± 0.03 (mg/g) on glucose after 48 h in baffled shake flasks. To improve the terminal alkene production, we identified and overcame the electron transfer limitation in $OleT_{MC}$, by introducing a two-component redox system, consisting of a putidaredoxin reductase CamA and a putidaredoxin CamB from *Pseudomonas putida,* into EcNN101, and demonstrated the terminal alkene production increased ~2.8 fold after 48 h. Overall, this study provides a better understanding of the function of P450 FA decarboxylases and helps guide future protein and metabolic engineering for enhanced microbial production of target designer alkenes in a recombinant host.

47 **Keywords**: P450 decarboxylase; terminal alkene; OleT; protein homology modeling; alanine
48 scan; residue scan; MOE; CamA; CamB; *Escherichia coli*; *Macrococcus caseolyticus*.

49

50

1. INTRODUCTION

Alkenes (or olefins) are industrially important platform chemicals used to manufacture polymers, lubricants, surfactants, and coatings (1). Alkenes are currently produced by the well-established chemical conversion route (e.g., hydrogen cracking) using petroleum-based feedstocks that are neither renewable nor sustainable (2, 3). In recent years, there is great interest in developing microbial conversion routes to produce alkenes from renewable and sustainable sources, such as biomass-derived fermentable sugars (4-10).

Various species are known to produce alkenes endogenously via decarbonylation of aldehydes (11-13), decarboxylation of FAs (14), condensation of unsaturated polyenes (15), and oxidation of FAs (7, 8). Various types of alkenes can be synthesized including alkadienes (16, 17), terminal alkenes (or 1-alkenes) (4, 6-8) as well as non-terminal alkenes (5), depending on enzyme types and substrates employed. To date, a number of different classes of enzymes have been reported to synthesize terminal alkenes including a P450 FA decarboxylase/peroxygenase (OleT, belonging to the CYP152 family) (4), a type-I polyketide synthase-like enzyme (CurM/Ols) (6), a desaturase-like enzyme (UndB) (7), and a non-heme oxidase (UndA) (8). These enzymes take various substrates (e.g., FAs, fatty aldehydes, or FA thioesters) to produce terminal alkenes with different carbon chain lengths. For instance, OleT, CurM/Ols, and UndB are capable of synthesizing (C_6-C_{12}) medium-chain and (> C_{12}) long-chain alkenes while UndA only produces medium chain length alkenes. The diversity of these enzyme specificities can potentially offer unique opportunities to develop microbial cell factories to engineer designer olefins for tailored applications.

Among the putative P450 FA decarboxylases/peroxygenases discovered, $OleT_{JE}$ is the most well-characterized enzyme that is capable of using either H_2O_2−dependent or H_2O_2−independent (O_2-dependent) mechanisms for alkene biosynthesis (4, 16, 18, 19). $OleT_{JE}$ has broad substrate specificity for C12:0-C20:0 FAs *in vitro*, with the highest towards C12:0

FA in the presence of redox partner proteins and C14:0 FA in the H_2O_2−dependent system (16). For the low-cost, large-scale production of terminal alkenes, the use of H_2O_2-independent decarboxylases (e.g., $OleT_{JE}$) is likely favorable by avoiding the external supply and cytotoxicity of H_2O_2. Thus, harnessing the enzyme library of H_2O_2−independent decarboxylases are important for the microbial production of terminal alkenes from biomass-derived sugars.

In this study, we expanded the library of unique OleTs for terminal alkene biosynthesis by characterizing a novel P450 FA decarboxylase $OleT_{MC}$ derived from *Macrococcus caseolyticus* for its catalytic functions. We employed protein homology modeling, *in silico* residue mutation analysis, and docking simulation to elucidate the underlying mechanism of fatty acid specificity of $OleT_{MC}$. Furthermore, we harnessed this $OleT_{MC}$ to engineer a terminal alkene biosynthesis pathway in *E. coli* for direct conversion of fermentable sugars into medium and long chain terminal alkenes (Figure 1). We discovered that electron transfer was the rate limiting step of alkene biosynthesis in the recombinant *E. coli*. This limitation could be alleviated by expressing the redox system CamA/B from *Pseudomonas putida* in the recombinant *E. coli*, resulting in enhanced alkene production.

2. RESULTS AND DISCUSSION

2.1 Genome mining of OleT decarboxylases for terminal alkene biosynthesis

To identify the putative H_2O_2-independent P450 FA decarboxylases, we performed a genome mining, a combination of the sequence alignment and phylogenetic analysis, using the protein sequence of $OleT_{JE}$ (ADW41779) as a template. The sequences of the CYP152 P450 enzyme family (4) were first aligned to select the candidates that have the conserved catalytic site residues Phe79, His85, and Arg245 like $OleT_{JE}$ (20). Among the 29 decarboxylase candidates, we found that three P450 enzymes from *M. caseolyticus* (WP_041635889.1), *Corynebacterium*

efficiens (WP_011075937.1), and *Kocuria rhizophila* (WP_012399225.1) have the conserved catalytic site residues (Supplementary Figure S1). Based on the phylogenetic analysis, we found that the P450 enzyme of *M. caseolyticus* (WP_041635889.1) is the closest ortholog to $OleT_{JE}$ with the highest amino acid identity (~60%) (Figure 2 and Supplementary Figure S1). Thus, we chose the P450 from *M. caseolyticus*, named $OleT_{MC}$, for further characterization.

2.2 *In vitro* characterization of $OleT_{MC}$

The expression of $OleT_{MC}$ in BL21 (λDE3) pNN33 was confirmed *in vivo* with reddish cell cultures due to the heme-containing $OleT_{MC}$ and *in vitro* by a sodium dodecyl sulfate polyacrylamide gel electrophoresis (SDS-PAGE) and spectrophotometric analysis (Supplementary Figure S2). After protein isolation, we performed the *in vitro* enzyme assay to examine the H_2O_2-independent decarboxylase activity of $OleT_{MC}$ towards linear, saturated FAs. The result shows that $OleT_{MC}$ could convert C10:0-C18:0 FAs to the corresponding odd chain terminal alkenes without H_2O_2 as an oxidant, confirmed by GC/MS (Supplementary Figure S3). Under the H_2O_2-independent (O_2-denpendent) conditions, $OleT_{MC}$ showed the highest specific activity towards C18:0 FA (1.13 ± 0.09 μM/min/mg) and the lowest specific activity towards C10:0 FA (0.17 ± 0.04 μM/min/mg) (Figure 3A). $OleT_{MC}$ exhibited almost the same specific activity for C12:0 FA (0.62 ± 0.10 μM/min/mg) and C14:0 FA (0.66 ± 0.04 μM/min/mg). We did not observe the activity of $OleT_{MC}$ for < C10:0 FAs. The FA specificity of $OleT_{MC}$ can be ranked as follows: C18:0 > C16:0 > C14:0 ≥ C12:0 > C10:0. Taken altogether, $OleT_{MC}$ is a potential FA decarboxylase for developing the terminal alkene biosynthesis pathway in recombinant hosts (e.g., *E. coli*) for direct conversion of fermentable sugars to terminal alkenes.

2.3 Elucidate the underlying mechanism governing the substrate specificity of $OleT_{MC}$

126 Currently, it is not well understood why different FA decarboxylases have different
127 substrate specificities. For instance, $OleT_{JE}$ prefers C12:0-C14:0 FAs to longer ones (16, 20)
128 while $OleT_{MC}$ favors C16:0-C18:0 FAs more than shorter ones (this study). To better
129 understand the underlying mechanism for governing the observed substrate preference of
130 $OleT_{MC}$, we focused on analyzing its protein structure, using protein homology modeling, *in*
131 *silico* residue mutation analysis, and docking simulation in combination with direct
132 experimental evidence.
133
134 **2.3.1** ***Analysis of the effect of catalytic site on the substrate specificity of*** $OleT_{MC}$.
135 Since $OleT_{MC}$ and $OleT_{JE}$ have different substrate preferences, we first tested whether structural
136 difference of their catalytic sites might exist and play a role. To do this, we built a 3D structure
137 of $OleT_{MC}$ using the version 2015.10 Molecular Operating Environment (MOE) software (21),
138 based on the best-hit crystallographic structure of the substrate-bound (C20:0, arachidic acid)
139 form of $OleT_{JE}$ (PDB:4L40 (19), ~60% amino acid identity) as a template. The Ramachandran
140 plot of $OleT_{MC}$ showed less than 0.5% of the residues to be in disallowed regions
141 (Supplementary Figure S4). Next, we superposed the heme-bound 3D structures of $OleT_{MC}$ and
142 $OleT_{JE}$ and found that they look almost identical (Figure 4A) with a very similar catalytic site
143 configuration (Figure 4B). This result suggests that other factors, not the catalytic site, might
144 be responsible for modulating the substrate specificities of $OleT_{MC}$ and $OleT_{JE}$. This
145 observation concurs with recent experimental evidence that single site directed mutations on
146 the catalytic site residues, including Phe79, His85, and Arg245, did not improve the catalytic
147 activity or change the substrate preference of $OleT_{JE}$ (20, 22, 23). Further, a recent molecular
148 dynamics study suggests several residues of $OleT_{JE}$ interacting with FA could significantly
149 contribute to the substrate binding free energy (24).
150

2.3.2 *Effect of binding free energy of OleT$_{MC}$ on its substrate preferences.* To examine whether the binding free energy of FA-bound OleT$_{MC}$ might affect its substrate specificity, we docked OleT$_{MC}$ with various FAs (C10:0-C18:0) in MOE. Our result shows that the FA-bound OleT$_{MC}$ complexes exhibited the interactions between FAs and OleT$_{MC}$ where the binding pocket of OleT$_{MC}$ contains greasy residues such as alanine (Ala, A), valine (Val, V), leucine (Leu, L), isoleucine (Ile, I), proline (Pro, P), phenylalanine (Phe, F) (Supplementary Figures S5 and S6). The binding free energies of different FA-bound OleT$_{MC}$ complexes increase with shorter chain FAs (Figure 3B). Remarkably, there is a strong linear correlation (R^2 = 0.92) between the binding free energies and specific activities of *OleT$_{MC}$* for various FAs (Figure 3C).

2.3.3 *Residues at the tail of FA binding site are critical for determining the substrate specificity of OleT$_{MC}$.* To identify the critical residues of the binding pocket that might affect the substrate specificity of OleT$_{MC}$, we first performed the alanine scan using the "alanine scan" tool in MOE. We scanned a set of 21 residues located at the FA docking sites of FA-bound OleT$_{MC}$ complexes (Supplementary Figure S5A) by substituting each candidate with Ala residue. Regardless of C10:0-C18:0 FAs, we found that the mutation at P72A or I171A increased the stability, while F174A or F296A decreased the stability (Figure 3D). In contrast, the mutation at I177A or V294A showed different stabilities for different FAs. Based on this first round of alanine scan and stability analysis, we narrowed the initial large set of 21 candidate residues to the 6 promising candidates, including P72, I171, F174, I177, F296 or V294, that might have a significant role for the substrate specificity of OleT$_{MC}$.

Next, we performed a comprehensive residue scan for these 6 candidate residues using the "residue scan" tool in MOE. Specifically, we generated a set of 54 OleT$_{MC}$ variants by systematically substituting each candidate with nine different hydrophobic residues including

176 glycine (Gly, G), Ala, Val, Leu, Ile, Pro, Phe, methionine (Met, M), and tryptophan (Trp, W)
177 and performed the stability analysis (Supplementary Figures S7A-F). By determining the
178 largest △stability differences between C18:0 FA-bound and C10:0 FA-bound $OleT_{MC}$
179 complexes for each $OleT_{MC}$ variant, we could select a list of the top five mutants, including
180 I177W, P72M, F296W, I177F, and P72F (Supplementary Figure S7G), for detail structure
181 analysis. Interestingly, all these five $OleT_{MC}$ variants, selected by combination of alanine and
182 residue scans, had the mutated residues located at the tail of the FA binding pocket (Figures
183 4C-4H).

184 To determine whether the top 5 $OleT_{MC}$ variants are responsible for substrate
185 preferences of $OleT_{MC}$, we next generated their 3D structures in MOE, followed by docking
186 simulation of these variants with various FAs (C10:0-C18:0). Our result shows that the two
187 variants, $OleT_{MC}$ P72M and F296W, significantly shifted substrate preferences while the other
188 variants, $OleT_{MC}$ I177W, I177F, and P72F, did not (Figure 4B). For the $OleT_{MC}$ F296W model,
189 we observed that the correct docking poses, whose Arg246 should interact with the carboxylic
190 functional group of FAs via hydrogen bonding, were no longer detected with C16:0 and C18:0
191 FAs. It has the lowest ΔG_{bind} of -8.43 kcal/mol with C14:0 FA and the highest ΔG_{bind} of -6.72
192 kcal/mol with C10:0 FA. Likewise, $OleT_{MC}$ P72M showed the lowest ΔG_{bind} of -8.23 kcal/mol
193 with C14:0 FA and the highest ΔG_{bind} of -6.18 kcal/mol with C18:0 FA. These results suggest
194 that P72M and F296W variants can shift the substrate preferences from longer to shorter FAs.
195
196 **2.3.4** ***Reconfiguration of the binding pocket is responsible for shifting the substrate***
197 ***preference in*** **$OleT_{MC}$ variants**. To elucidate the underlying mechanism for shifting the
198 substrate preference of $OleT_{MC}$, we compared the structures of $OleT_{MC}$ variants, including
199 I177W (Figure 4D), P72M (Figure 4E), F296W (Figure 4F), I177F (Figure 4G), and P72F
200 (Figure 4H), and its wildtype (Figure 4C). Our result shows that the disruption of the FA

binding pockets affected substrate preferences of $OleT_{MC}$ P72M (Figure 4E) and F296W (Figure 4F). Specifically, they interfered with the access and docking of the longer C16:0-C18:0 FAs. Furthermore, since $OleT_{MC}$ F296W could not dock C16:0 and C18:0 FAs but $OleT_{MC}$ F72M could, it implies that the size of mutated residue (e.g. Trp (W) having a larger size than Met (M)) can play a significant role in changing the substrate specificity of $OleT_{MC}$.

Taken altogether, the residues at the tail of FA binding pocket of $OleT_{MC}$, such as P72 and F296, are critical for determining the substrate specificity of $OleT_{MC}$. Mutating these residues, instead of those at the catalytic site, can provide a promising protein engineering strategy to shift substrate specificity of $OleT_{MC}$.

2.4 Establishing the terminal alkene biosynthesis pathway in *E. coli*

We designed the heterologous terminal alkene biosynthesis pathway in *E. coli* BL21 (λDE3), consisting of two genes − the leaderless *tesA** gene encoding a thioesterase to convert acyl ACPs to FAs and the $OleT_{MC}$ gene encoding a decarboxylase to convert these FAs to terminal alkenes. We chose TesA* because it has higher specificities towards C16:0-C18:0 acyl ACPs than C12:0-C14:0 acyl ACPs (25) to produce corresponding FAs that are preferable substrates for $OleT_{MC}$. Figure 5A-C shows kinetics of cell growth, sugar consumption, and product formation in shake flask experiments of the recombinant *E. coli* EcNN101 engineered to carry the terminal alkene biosynthesis pathway.

During the first 24 h of growth phase, EcNN101 could grow and produce odd terminal alkenes. At 24 h, cells completely consumed 20 g/L of glucose and entered the stationary phase with a biomass titer of 4.16 ± 0.07 g/L (Figure 5A). Terminal alkene production peaked at a titer of 21.92 ± 0.69 mg/L, comprised of 4.5% ± 0.2% C11 alkene, 38.9% ± 1.1% C13 alkene, 55.4% ± 0.8% C15 alkene, and 1.2% ± 0.5% C17 alkene (Figure 5B). Besides alkenes, the corresponding FAs were also produced at a much higher titer of 558.03 ± 18.95 mg/L,

consisting of 24.9% ± 0.1% C12:0 FA, 41.0% ± 0.2% C14:0 FA, 25.2% ± 0.4% C16:0 FA, 7.6% ± 0.3% C18:0 FA, and 1.4% ± 0.1% C20:0 FA (Figure 5C). The composition of these FAs correlated well with the specificity of TesA* (25). The relatively high FA production clearly implied that $OleT_{MC}$ was the rate-limiting step of the engineered terminal alkene biosynthesis pathway. The result also shows that the C15 alkene was produced at the highest level even though the fraction of C16:0 FA was lower than that of C14:0 FA and relatively similar to that of C12:0 FA. This result is consistent with the substrate preference of $OleT_{MC}$ towards C16:0 FA characterized *in vitro* and also implies that C16:0 FA was not limiting for decarboxylation. The production of C17 terminal alkene, however, was relatively low likely due to the low availability of C18:0 FA.

During the stationary phase (after 24 h), no glucose was available and about 398.15 ± 4.79 mg/L saturated FAs were consumed primarily for cell maintenance while cell concentration remained relatively constant. At 48 h, the alkene titer was slightly decreased to 17.78 ± 0.63 mg/L probably due to cell lysis and/or evaporation. The final alkene yield was 0.87 ± 0.03 mg/g. It is interesting to notice that EcNN101 did not produce terminal alkenes during stationary phase even though degradation of saturated FAs, highly reduced substrates, could generate available NAD(P)H for FA decarboxylation via the β-oxidation pathway. This result implies that olefin production might be limited by the efficiency of electrons transferred to $OleT_{MC}$ for decarboxylation.

2.5 Improving terminal alkene production by enhancing electron shuttling to $OleT_{MC}$

It is known that the electron flow from NAD(P)H to the terminal P450 enzyme is facilitated by a two-component redox system such as ferredoxin reductase (FDR) and NAD(P)H-dependent ferredoxin (FDX). Most of the bacterial P450s belonging to the class I P450s use this two-component redox system for shuttling electrons (26, 27). We hypothesized that the $OleT_{MC}$

activity in EcNN101 might have been limiting during the stationary phase due to the lack of a two-component redox system. To test this hypothesis, we constructed EcNN201 that contains both the terminal alkene biosynthesis pathway and a two-component redox system well-characterized for *E. coli*. This redox system consists of an NAD(P)H-dependent putidaredoxin reductase (CamA) and a [2Fe–2S] putidaredoxin (CamB) transferring two electrons, one at a time, from NAD(P)H to the P450 enzyme (26-28).

Like EcNN101, EcNN201 could produce terminal alkenes during the growth phase (Figure 5E). At 24 h, EcNN201 reached a cell concentration of 5.29 ± 0.05 g/L and entered the stationary phase after completely consuming 20 g/L glucose (Figure 5D). EcNN201 produced 19.25 ± 2.03 mg/L terminal alkenes, comparable to EcNN101. The composition of terminal alkenes produced by EcNN201 comprised of 2.4% ± 1.5% C11 alkene, 32.1% ± 5.8% C13 alkene, 64.3% ± 6.7% C15 alkene, and 1.2% ± 0.3% C17 alkene. Like EcNN101, EcNN201 produced a high amount of saturated FAs (556.12 ± 4.44 mg/L) consisting of 17.3% ± 0.3% C12:0 FA, 40.0% ± 0.5% C14:0 FA, 33.3% ± 0.3% C16:0 FA, 7.8% ± 0.4% C18:0 FA, and 1.6% ± 0.3% C20:0 FA (Figure 5F). Overall, the terminal alkene production phenotypes were similar between EcNN101 and EcNN201 during the growth phase. This result implies that reducing equivalents were primarily channeled for ATP generation and biomass synthesis that are thermodynamically favorable under aerobic conditions, and hence likely became limited for decarboxylation to produce target alkenes.

However, during the stationary phase where glucose was not available, EcNN201 consumed a total amount of 407.45 ± 22.19 mg/L FAs for not only cell maintenance but also terminal alkene production. The terminal alkene production was increased up to 58% higher during the stationary phase than the growth phase, underlying the critical functional role of the redox system responsible for enhanced terminal alkene production. EcNN201 produced up to 49.64 ± 1.33 mg/L terminal alkenes, consisting of 0.7% ± 0.1% C11 alkene, 26.4% ± 2.6%

C13 alkene, 70.7% ± 3.0% C15 alkene, and 2.2% ± 0.4% C17 alkene. At 48 h, the alkene titer and yield were 49.64 ± 1.33 mg/L and 2.44 ± 0.06 mg/g, respectively. In comparison to EcNN101, the terminal alkene production of EcNN201 increased by 2.8 fold. It is interesting to observe that C12:0-C14:0 FAs were primarily degraded for cell maintenance and C16:0 FA utilized for alkene biosynthesis based on the FA distributions at 24 and 48 h (Figure 5F). This degradation phenotype is consistent with the distribution of terminal alkenes as well as the substrate preference of the endogenous FA synthetase FadD of *E. coli* responsible for catalyzing the first step of the β-oxidation (29).

The FA decarboxylation was clearly the rate-limiting step in our engineered terminal alkene biosynthesis pathway due to high accumulation of saturated FAs observed during the growth phase. The main cause of limited decarboxylation is inefficient electron transfer. We can observe that EcNN101 could not produce terminal alkenes during this stationary phase due to lack of the electron transfer to $OleT_{MC}$. This limitation could be overcome by introducing the two-component redox system in EcNN201. Specifically, the FA degradation during the stationary phase in EcNN201 generated high levels of reducing equivalents (i.e. NAD(P)H) via β-oxidation, and the redox system helped channel electrons to $OleT_{MC}$, thereby improving terminal alkene production.

EcNN201 produced terminal alkenes at a very comparable level to the recombinant *E. coli* harnessing the $OleT_{JE}$ decarboxylase from *Jeotgalicoccus sp.* (16). In our study, we did not observe EcNN101 and EcNN201 producing alkadienes even though unsaturated FAs were produced (Supplementary Figure S8). Because the current terminal alkene production in EcNN201 is very inefficient, improving carbon and electron fluxes via metabolic engineering is critical for enhanced terminal alkene production in future study. In addition, controlling environmental conditions (e.g., sufficient supply of oxygen and use of highly reduced substrates) can potentially help improve terminal alkene production.

3. CONCLUSION

In this study, we discovered and characterized a novel P450 FA decarboxylase $OleT_{MC}$ for H_2O_2-independent biosynthesis of odd-chain, terminal alkenes. By combining the homology modeling, *in silico* residue mutation analysis, and docking simulation with direct experimental evidence, we elucidated the underlying mechanism that determines the substrate preferences of $OleT_{MC}$. In addition, we demonstrated the direct biosynthesis of medium- and long-chain terminal alkenes in an engineered *E. coli* from fermentable sugars, abundant from lignocellulosic biomass. We found that the inefficient electron transfer in $OleT_{MC}$ was the rate limiting step that could be overcome by introducing a two-component redox system. Our results help lay out a foundation for future study to modulate fatty acid thioesterases and Ole_{TM} specificities to produce designer terminal alkenes with desirable carbon chain characteristics. Overall, this study provides a better understanding of the novel functions of FA decarboxylases and helps guide future protein and metabolic engineering for enhanced terminal alkene production in a recombinant host.

4. MATERIALS AND METHODS

4.1 Bacterial strains and plasmids

Table 1 shows a list of bacterial strains and plasmids used in this study. *E. coli* TOP10 was used for molecular cloning while BL21 (λDE3) was employed as an expression and characterization host. All plasmids were constructed by using a modified pETite* (30), a derivative of pETite C-His backbone vector (Lucigen Corp., WI, USA), suitable for the BglBricks gene assembly method (31). Primers used to construct the plasmids in this study are listed in Table 2.

To construct the plasmid pCT71, the leaderless *tesA** was amplified from the genomic DNA of *E. coli* MG1655 using the primers mw.24f/p064_r, and inserted into pETite* via the

NdeI/XhoI sites. The gene *tesA** was derived from *tesA* whose leader peptide sequence was removed to keep the encoded protein TesA* localized in the cytosol (32). The plasmid pNN33 was constructed by the Gibson gene assembly method (33) using 2 DNA fragments: i) the decarboxylase gene $OleT_{MC}$ amplified from the genomic DNA of *M. caseolyticus* using the primers Nhis6_$OleT_{MC}$F/Nhis6_$OleT_{MC}$R and ii) the backbone fragment amplified from pETite* using the primers pnn33_Nhis6F/pnn33_Nhis6R. To construct the plasmid pNN32, $OleT_{MC}$ was amplified using the primers mc_decarbF/rev_decarb and inserted into pCT71 via the BamHI/XhoI sites. The plasmid pNN34 was constructed by the Gibson gene assembly method using 3 DNA fragments: i) *camA* gene amplified from the genomic DNA of *P. putida* using the primers pnn82/pnn83, ii) *camB* amplified from the genomic DNA of *P. putida* using the primers pnn84/pnn85, and iii) the backbone fragment amplified from pETite* using the primers pETiteF/pETiteR. All plasmid constructs were confirmed by enzyme digestion, PCR amplification of the respective genes, and sequencing.

The strain EcNN101 was generated by introducing pNN32 into BL21 (λDE3) via electroporation. Similarly, the strain EcNN201 was created by co-transforming pNN32 and pNN34 into BL21 (λDE3).

4.2 Medium and strain characterization

Medium. For molecular cloning and protein expression, Luria-Bertani (LB) medium containing 5 g/L yeast extract, 10 g/L tryptone, 5 g/L NaCl, and antibiotics (if applicable) was used for *E. coli* and *P. putida* cultures. The medium for cultivating *M. caseolyticus* was comprised of 5 g/L glucose, 5 g/L yeast extract, 10 g/L casein peptone, and 5 g/L NaCl. The hybrid M9 medium used for strain characterization contained 1X M9 salt solution (34), 1 mM $MgSO_4$, 10 mM $CaCl_2$, 1 mL/L stock trace metals solution, 5 g/L yeast extract, 20 g/L glucose, and appropriate antibiotics (e.g., 50 μg/mL kanamycin or 100 μg/mL ampicillin for single

plasmid selection or 25 μg/mL kanamycin plus 50 μg/mL ampicillin for double plasmid selection) (35).

Strain characterization. For terminal alkene production experiments, single colonies were inoculated in 15 mL tubes containing 8 mL of LB medium and incubated in a rotary shaker at 37°C with a shaking rate of 175 rpm for 12 hour (h). The overnight seed culture was then transferred into the hybrid M9 medium with an initial OD_{600nm} ~0.05 in 500 mL baffled shake flasks with a 100 mL working volume. When reaching the exponential phase of OD_{600nm} ~0.6, the cell culture was first supplemented with 1 mM 5-aminolevulinic acid (ALA) to enhance the yield of active P450 (36), followed by IPTG induction at a working concentration of 0.5 mM, and run for a total of 48 h. Samples were collected for determining cell growth, substrate consumption, and product formation. All experiments were performed in biological triplicates.

4.3 Enzyme expression, purification, and characterization

BL21 (λDE3) pNN33 was used to express $OleT_{MC}$ His-tagged at the N-terminus in LB medium at 20 celcius (°C). Exponentially grown cells (OD_{600nm} ~0.6) were induced with IPTG at a working concentration of 0.5 mM. After 20 h, cells were collected, washed, and resuspended in 50 mM phosphate buffer (pH 7.5). The resuspended cells were disrupted by ultrasonication with a sonic dismembrator (Model # FB120, Thermo Fisher Scientific Inc., MA, USA) and then centrifuged at 13,500 rcf for 20 min at 4°C to collect the soluble crude cell extract for downstream protein purification. The sonication protocol was set with 70% amplitude with cycles of 5 second ON/10 second OFF pulses on ice for 15 minutes.

The expressed $OleT_{MC}$ protein was semi-purified by the HisPur Ni-NTA Spin column (cat # PI88224, Thermo Fisher Scientific, MA, USA) according to the manufacturer's instruction. Following incubation for 1 h at 4°C, the resin was washed three times with wash

buffer (20 mM of imidazole) and the His-tagged $OleT_{MC}$ was eluted from the resin by adding elution buffer (500 mM of imidazole). Then, the final protein sample was concentrated using Amicon Ultra centrifugal filters (cat # UFC801024, Merck, NJ, USA). The purified protein was analyzed by the 12% SDS-PAGE and the protein concentration was determined by the Bradford assay (37).

To quickly test the active form of $OleT_{MC}$ (i.e., the actual heme content of P450 protein), the spectrophotometric carbon monoxide (CO) difference spectral analysis was routinely carried out to determine the maximum characteristic absorbance at 450 nm (38). First, 0.5 mL of 20 mg/mL purified protein sample was diluted in 4.5 mL of 50 mM Tris-HCl buffer (pH 7.6) containing 1 mM EDTA and 10% (v/v) glycerol. The solution was then supplemented with a few crystals of sodium dithionite and saturated with ~30-40 bubbles of CO at a rate of 1 bubble per second. The maximum spectrophotometric absorbance peak at 450 nm indicates the reduced P450 complexed with CO and hence confirms the enzymatic catalytic center of $OleT_{MC}$ is active.

The H_2O_2-independent FA decarboxylase activity of $OleT_{MC}$ was characterized *in vitro* with various linear, saturated C8:0-C20:0 FAs. Each reaction assay has a working volume of 500 µL that contained 1 mM NADH, 10 µM spinach ferredoxin (cat. # F3013, Sigma Aldrich, CA, USA), 0.5 unit spinach ferredoxin reductase (cat. # F0628, Sigma Aldrich, CA, USA), 20 µg/mL purified $OleT_{MC}$, and 0.05 mM FAs. The assay was conducted at 37ºC for 60 min. After the reaction, alkenes were extracted with ethyl acetate, and analyzed by gas chromatography coupled with mass spectrometry.

4.4 Analytical methods

399 *Cell growth.* Cell optical density was measured at OD_{600nm} using a spectrophotometer
400 (Spectronic 20+, Thermo Fisher Scientific, MA, USA). The correlation between the cell optical
401 density and dry cell weight (DCW) was determined to be 1 OD_{600nm} = 0.48 g DCW/L.
402 *High performance liquid chromatography (HPLC).* The HPLC Shimadzu system
403 equipped with a BioRad Aminex HPX 87-H column (cat # 1250140, BioRad, CA, USA) and
404 both RID and UV-VIS detectors (Shimadzu Scientific Instruments, Inc., MD, USA) were used
405 to quantify extracellular metabolites (e.g., glucose, organic acids, and alcohols). The running
406 method used 10 mN H_2SO_4 as a mobile phase operated at a flow rate of 0.6 mL/min and an
407 oven temperature set at 48°C (39).
408 *Gas chromatography coupled with mass spectroscopy (GC/MS).* For FAs analysis,
409 sample preparation and GC/MS methods were described previously (40). For terminal alkene
410 analysis, 500 µL of samples (cells plus supernatants) were transferred to a 2 ml polypropylene
411 microcentrifuge tube with a screw cap containing 100-200 mg of glass beads (0.25-0.30 mm
412 in diameter), 60 µL of 6 N HCl, and 500 µL of ethyl acetate solution containing 1 mg/L of ethyl
413 pentadecanoate as an internal standard. The cells were lysed by bead bashing for 4 min using
414 a Biospec Mini BeadBeater 16 and then centrifuged at 13,300g for 2 min. The extractants of
415 the organic layer were used for the GC/MS analysis. All alkenes were analyzed by using
416 HP6890 GC/MS system equipped with a 30 m x 0.25 mm i.d. 0.25 µm film thickness column
417 plus an attached 10 m guard column (Zebron ZB-5, Phenomenex Inc.) and a HP 5973 mass
418 selective detector. An electron ionization in scan mode (50 to 650 m/z) method was deployed
419 to analyze 1 µL of samples. The column temperature was initially held at 50°C for 1 min,
420 increased by 20°C/min until 300°C, and held for 2 min. Helium was used as a carrier gas and
421 run at 1 mL/min. The mass transfer line and ion source were set at 250°C and 200°C,
422 respectively.
423

4.5 Bioinformatics

For sequence alignment and phylogenetic analysis, protein sequences were retrieved from the National Center for Biotechnology Information (NCBI), and were inputted into MEGA7 (41) and aligned via MUSCLE (42). The phylogenetic tree was generated using the neighbor-joining algorithm with a 1000 bootstrap value. BLASTp was used to calculate the identity of sequences (43) using $OleT_{JE}$ as the template.

4.6 Homology modeling and *in silico* analysis of $OleT_{MC}$

Homology modeling. The homology model of $OleT_{MC}$ was generated using the version 2015.10 Molecular Operating Environment (MOE) software (21). To obtain the heme-bound protein structure, the reference substrate, heme, was first extracted from the best hit, substrate-bound crystallographic structure of $OleT_{JE}$ (PDB:4L40) and then added to the homology model of $OleT_{MC}$. Next, the heme-bound model of $OleT_{MC}$ generated was optimized by energy minimization using the Amber10:EHT (Extended Huckel Theory) force field (44, 45). The Ramachandran plot analysis was performed to determine the overall stereochemical property of the protein model.

Docking simulation. To dock various FAs with the heme-bound homology model of $OleT_{MC}$, the 3D structures of various C10:0-C18:0 FAs were first generated by modifying C20:0 FA extracted from $OleT_{JE}$ (PDB:4L40) with the '3D builder' tool of MOE and then optimized by energy minimization using the Amber10:EHT force field. Next, the "site finder" tool of MOE was used to search for potential binding sites. Upon identifying the site consistent with the reported catalytic site of $OleT_{JE}$ (20), dummy atoms were generated to mark potential binding sites. To select the exclusive potential binding site of FA, we also removed some dummy atoms located near heme. Finally, we added the target C10:0-C18:0 FAs to the binding

448 site of the heme-bound homology model of $OleT_{MC}$. All structures were protonated using the
449 "protonate3D" tool of MOE prior to docking simulation.

450 Docking simulations were carried out as previously described (46). In brief, the induced
451 fit docking protocol employed the Triangle Matcher placement method and the London △G
452 scoring function. In our docking simulations, we performed 30 docking interactions for each
453 FA substrate. The binding free energy ($\triangle G_{bind}$, in kcal/mol) for each binding pose was then
454 minimized using the Amber10:EHT force field and rescored with the GBVI/WSA △G scoring
455 function (44). The best scored pose, exhibiting the crucial interaction between the residue
456 Arg246 and carboxylic functional group of the substrate via hydrogen bonding (20) at root-
457 mean-square-deviation (RMSD) < 2 Å, was selected for further analysis. The "surface and
458 maps" tool of MOE was employed to visualize the molecular surface of atoms in the potential
459 FA binding site.

460 *In silico mutation analysis.* The "alanine scan" and the "residue scan" tools in MOE
461 were used for *in silico* mutation analysis of FA-$OleT_{MC}$ complexes. Specifically, the alanine
462 scanning technique (47, 48) was employed to determine the importance of a specific residue to
463 the stability, affinity, and/or property of the FA-$OleT_{MC}$ complexes upon being substituted with
464 Ala in the binding pocket. Residue scanning technique, also known as site-directed
465 mutagenesis (49), was applied to generate large number of $OleT_{MC}$ variants for the
466 comprehensive mutation study using the selected residues from the alanine scan. By utilizing
467 these tools, we could replace each of the interface residues with a specific residue of interest
468 and calculates the effect of the mutation on the binding free energy ($\triangle G_{bind}$) of the complexes.
469 The △Stability values (kcal/mol) were calculated as the relative binding free energy difference
470 ($\triangle\triangle G_{bind}$) between the mutant ($\triangle G_{mutant}$) and wild type ($\triangle G_{wildtype}$) in MOE.

ACKNOWLEDGEMENTS

We would like to thank Dr. Fu-min Menn (Center of Environmental Biotechnology, UTK) for his assistance in developing the GC/MS method, Dr. Jerome Baudry (UTK) for accessing the MOE software, Dr. Donovan Layton (UTK) for assistance with GC/MS and bioinformatics analyses, and members of Trinh lab for proofreading and providing critical comments on the manuscript.

FUNDING

This research was supported by the laboratory start-up, SEERC, and JDRD seed funds from the University of Tennessee, Knoxville (UTK), a NSF CAREER award (NSF#1553250 to CTT), and a DOE subcontract grant (DE-AC05-00OR22725) by the Center of Bioenergy Innovation (CBI), the U.S. Department of Energy Bioenergy Research Center funded by the Office of Biological and Environmental Research in the DOE Office of Science.

Conflict of interest statement: None declared

REFERENCES

1. Lappin GR, Sauer JD. 1989. Alpha Olefins Applications Handbook, vol 37. CRC Press.

2. Ren T, Patel M, Blok K. 2006. Olefins from conventional and heavy feedstocks: Energy use in steam cracking and alternative processes. Energy 31:425-451.

3. Mol J. 2004. Industrial applications of olefin metathesis. Journal of Molecular Catalysis A: Chemical 213:39-45.

4. Rude MA, Baron TS, Brubaker S, Alibhai M, Del Cardayre SB, Schirmer A. 2011. Terminal olefin (1-alkene) biosynthesis by a novel p450 fatty acid decarboxylase from *Jeotgalicoccus* species. Applied and Environmental Microbiology 77:1718-1727.

5. Beller HR, Goh E-B, Keasling JD. 2010. Genes Involved in Long-Chain Alkene Biosynthesis in Micrococcus luteus. Applied and Environmental Microbiology 76:1212-1223.

6. Mendez-Perez D, Begemann MB, Pfleger BF. 2011. Modular Synthase-Encoding Gene Involved in α-Olefin Biosynthesis in Synechococcus sp. Strain PCC 7002. Applied and Environmental Microbiology 77:4264-4267.

7. Rui Z, Harris NC, Zhu X, Huang W, Zhang W. 2015. Discovery of a Family of Desaturase-Like Enzymes for 1-Alkene Biosynthesis. ACS Catalysis 5:7091-7094.

8. Rui Z, Li X, Zhu X, Liu J, Domigan B, Barr I, Cate JHD, Zhang W. 2014. Microbial biosynthesis of medium-chain 1-alkenes by a nonheme iron oxidase. Proceedings of the National Academy of Sciences 111:18237-18242.

9. Chen B, Lee D-Y, Chang MW. 2015. Combinatorial metabolic engineering of Saccharomyces cerevisiae for terminal alkene production. Metabolic Engineering 31:53-61.

10. Zhu Z, Zhou YJ, Kang M-K, Krivoruchko A, Buijs NA, Nielsen J. 2017. Enabling the synthesis of medium chain alkanes and 1-alkenes in yeast. Metabolic Engineering 44:81-88.

11. Winters K, Parker P, Van Baalen C. 1969. Hydrocarbons of blue-green algae: geochemical signfficance. Science 163:467-468.

512 12. Tornabene T. 1982. Microorganisms as hydrocarbon producers, p 49-52, New Trends
513 in Research and Utilization of Solar Energy through Biological Systems. Springer.
514 13. Ladygina N, Dedyukhina E, Vainshtein M. 2006. A review on microbial synthesis of
515 hydrocarbons. Process Biochemistry 41:1001-1014.
516 14. Görgen G, Frößl C, Boland W, Dettner K. 1990. Biosynthesis of 1-alkenes in the
517 defensive secretions ofTribolium confusum (Tenebrionidae); stereochemical implications.
518 Experientia 46:700-704.
519 15. Ney P, Boland W. 1987. Biosynthesis of 1-alkenes in higher plants. European Journal
520 of Biochemistry 162:203-211.
521 16. Liu Y, Wang C, Yan J, Zhang W, Guan W, Lu X, Li S. 2014. Hydrogen peroxide-
522 independent production of α-alkenes by OleTJE P450 fatty acid decarboxylase. Biotechnol
523 Biofuels 7:28.
524 17. Mendez-Perez D, Herman NA, Pfleger BF. 2014. A Desaturase Gene Involved in the
525 Formation of 1, 14-Nonadecadiene in Synechococcus sp. Strain PCC 7002. Applied and
526 Environmental Microbiology 80:6073-6079.
527 18. Dennig A, Kuhn M, Tassoti S, Thiessenhusen A, Gilch S, Bülter T, Haas T, Hall M,
528 Faber K. 2015. Oxidative Decarboxylation of Short-Chain Fatty Acids to 1-Alkenes.
529 Angewandte Chemie International Edition 54:8819-8822.
530 19. Belcher J, McLean KJ, Matthews S, Woodward LS, Fisher K, Rigby SE, Nelson DR,
531 Potts D, Baynham MT, Parker DA. 2014. Structure and biochemical properties of the alkene
532 producing cytochrome P450 OleTJE (CYP152L1) from the Jeotgalicoccus sp. 8456
533 bacterium. Journal of Biological Chemistry 289:6535-6550.
534 20. Matthews S, Belcher JD, Tee KL, Girvan HM, McLean KJ, Rigby SE, Levy CW, Leys
535 D, Parker DA, Blankley RT, Munro AW. 2017. Catalytic Determinants of Alkene Production
536 by the Cytochrome P450 Peroxygenase OleTJE. J Biol Chem 292:5128-5143.

537 21. MOE. Molecular Operating Environment (MOE), Chemical Computing Group ULC,
538 1010 Sherbooke St. West, Suite #910, Montreal, QC, Canada, H3A 2R7.
539 22. Hsieh CH, Makris TM. 2016. Expanding the substrate scope and reactivity of
540 cytochrome P450 OleT. Biochem Biophys Res Commun 476:462-466.
541 23. Fang B, Xu H, Liu Y, Qi F, Zhang W, Chen H, Wang C, Wang Y, Yang W, Li S. 2017.
542 Mutagenesis and redox partners analysis of the P450 fatty acid decarboxylase OleTJE. Sci Rep
543 7:44258.
544 24. Du J, Liu L, Guo LZ, Yao XJ, Yang JM. 2017. Molecular basis of P450 OleT(JE): an
545 investigation of substrate binding mechanism and major pathways. Journal of Computer-
546 Aided Molecular Design 31:483-495.
547 25. Bonner WM, Bloch K. 1972. Purification and Properties of Fatty Acyl Thioesterase I
548 from Escherichia coli. Journal of Biological Chemistry 247:3123-3133.
549 26. Peterson J, Lorence M, Amarneh B. 1990. Putidaredoxin reductase and putidaredoxin.
550 Cloning, sequence determination, and heterologous expression of the proteins. Journal of
551 Biological Chemistry 265:6066-6073.
552 27. Gunsalus I, Sligar S. 1978. Oxygen reduction by the P450 monoxygenase systems.
553 Advances in Enzymology and Related Areas of Molecular Biology, Volume 47:1-44.
554 28. Green AJ, Munro AW, Cheesman MR, Reid GA, von Wachenfeldt C, Chapman SK.
555 2003. Expression, purification and characterisation of a Bacillus subtilis ferredoxin: a potential
556 electron transfer donor to cytochrome P450 BioI. Journal of inorganic biochemistry 93:92-99.
557 29. Kameda K, Nunn W. 1981. Purification and characterization of acyl coenzyme A
558 synthetase from Escherichia coli. Journal of Biological Chemistry 256:5702-5707.
559 30. Layton DS, Trinh, C.T. 2014. Engineering Modular Ester Fermentative Pathways in
560 *Escherichia coli*. Metab Eng 26:77-88.

561 31. Anderson JC, Dueber J, Leguia M, Wu G, Goler J, Arkin A, Keasling J. 2010.
562 BglBricks: A flexible standard for biological part assembly. Journal of Biological Engineering
563 4:1.
564 32. Cho H, Cronan JE. 1995. Defective Export of a Periplasmic Enzyme Disrupts
565 Regulation of Fatty Acid Synthesis. Journal of Biological Chemistry 270:4216-4219.
566 33. Gibson DG. 2009. Synthesis of DNA fragments in yeast by one-step assembly of
567 overlapping oligonucleotides. Nucleic Acids Research 37:6984-6990.
568 34. Sambrook J. 2001. Molecular Cloning: A Laboratory Manual. Cold Spring Harbor
569 Laboratory Press.
570 35. Trinh CT, Li J, Blanch HW, Clark DS. 2011. Redesigning Escherichia coli Metabolism
571 for Anaerobic Production of Isobutanol. Appl Environ Microbiol 77:4894-4904.
572 36. Jansson I, Stoilov I, Sarfarazi M, Schenkman JB. 2000. Enhanced expression of
573 CYP1B1 in Escherichia coli. Toxicology 144:211-219.
574 37. Bradford M. 1976. A rapid and sensitive method for the quantitation of microgram
575 quantitites of protein utilizing the principle of protein-dye binding. Analytical Biochemistry
576 72:248 - 254.
577 38. Omura T, Sato R. 1964. The carbon monoxide-binding pigment of liver microsomes. I.
578 Evidence for its hemoprotein nature. J Biol Chem 239:2370-2378.
579 39. Trinh CT, Unrean P, Srienc F. 2008. Minimal Escherichia coli cell for the most efficient
580 production of ethanol from hexoses and pentoses. Applied and Environmental Microbiology
581 74:3634-3643.
582 40. Wierzbicki M, Niraula N, Yarrabothula A, Layton DS, Trinh CT. 2016. Engineering an
583 Escherichia coli platform to synthesize designer biodiesels. J Biotechnol 224:27-34.
584 41. Kumar S, Stecher G, Tamura K. 2016. MEGA7: Molecular Evolutionary Genetics
585 Analysis Version 7.0 for Bigger Datasets. Molecular Biology and Evolution 33:1870-1874.

586 42. Edgar RC. 2004. MUSCLE: multiple sequence alignment with high accuracy and high
587 throughput. Nucleic Acids Research 32:1792-1797.
588 43. Altschul SF, Gish W, Miller W, Myers EW, Lipman DJ. 1990. Basic local alignment
589 search tool. Journal of Molecular Biology 215:403-410.
590 44. Corbeil CR, Williams CI, Labute P. 2012. Variability in docking success rates due to
591 dataset preparation. J Comput Aided Mol Des 26:775-86.
592 45. Case DA, Cheatham TE, 3rd, Darden T, Gohlke H, Luo R, Merz KM, Jr., Onufriev A,
593 Simmerling C, Wang B, Woods RJ. 2005. The Amber biomolecular simulation programs. J
594 Comput Chem 26:1668-88.
595 46. Liu M, Zheng N, Li D, Zheng H, Zhang L, Ge H, Liu W. 2016. cyp51A-based
596 mechanism of azole resistance in Aspergillus fumigatus: Illustration by a new 3D Structural
597 Model of Aspergillus fumigatus CYP51A protein. Med Mycol 54:400-8.
598 47. Massova I, Kollman PA. 1999. Computational alanine scanning to probe protein-
599 protein interactions: A novel approach to evaluate binding free energies. Journal of the
600 American Chemical Society 121:8133-8143.
601 48. Morrison KL, Weiss GA. 2001. Combinatorial alanine-scanning. Current Opinion in
602 Chemical Biology 5:302-307.
603 49. Eriksen DT, Lian JZ, Zhao HM. 2014. Protein design for pathway engineering. Journal
604 of Structural Biology 185:234-242.
605

606 **Table 1:** List of strains and plasmids

Strains/plasmids	**Genotype**	**Sources**
Strains		
P. putida	wildtype	ATCC17453
M. caseolyticus	wildtype	ATCC13548
TOP10	F^- mcrA Δ(mrr-hsdRMS-mcrBC) φ80lacZΔM15 ΔlacX74 nupG recA1 araD139 Δ(ara-leu)7697 galE15 galK16 rpsL(Str^R) endA1 λ^-	Invitrogen
BL21 (λDE3)	F^- ompT $hsdS_B$ (r_B^- m_B^-) gal dcm (λDE3)	Invitrogen
EcNN101	BL21 (λDE3) carrying pNN32	this study
EcNN201	BL21 (λDE3) carrying pNN32 and pNN34	this study
Plasmids		
pETite C-His	pBR322 *ori*; kan^R	Lucigen
pETite*	kan^R	Layton 2014
pCT71	pETite* p_{T7}::*tesA**::T_{T7}; kan^R	this study
pNN33	pETite* p_{T7}::*oleT*$_{MC}$::T_{T7}; kan^R	this study
pNN32	pETite* p_{T7}:: *tesA**::*oleT*$_{MC}$:: T_{T7}; kan^R	this study
pNN34	pETite* p_{T7}::*camAB*::T_{T7}; amp^R	this study

607

608

609 **Table 2:** List of primers

610

Primers	**Primer sequence (5' to 3')**
mw.24f	AAA AAA CAT ATG GCG GAC ACG TTA TTG ATT CT
p064_r	AAA AAA CTC GAG TTA GGA TCC TTA TGA GTC ATG ATT TAC TAA AG
Nhis6_OleT$_{MC}$F	AGA AGG AGA TAT ACA TAT GCA TCA TCA CCA CCA TCA CAG TAA AAG AGT TCC TAA AGA TAG
Nhis6_OleT$_{MC}$R	GTT ATG CTA GTT ATT GCT CAG CGG TGG CGG CCG CTC TAT TAT TTT GTA CGG TCG ATA TTC
pnn33_Nhis6F	TAA TAG AGC GGC CGC CAC
pnn33_Nhis6R	GTG ATG GTG GTG ATG ATG CAT ATG TAT ATC TCC TTC TTA TAG TTA AAC AAA ATT AT
mc_DecarbF	ATG GAT CCA AAA ATG AGG GTA GAG TTT ACT ATT AA
rev-Decarb	ATC TCG AGT TAT TTT GTA CGG TCG ATA TTC ACC CT
pnn82	ATA ATT TTG TTT AAC TAT AAG AAG GAG ATA TAC ATA TGA ACG CAA ACG ACA ACG TGG TC
pnn83	GAC ACA TAC ACT ACT TTA GAC ATT TAT ATC TCC TTT CAG GCA CTA CTC AGT TCA GCT TT
pnn84	AAA GCT GAA CTG AGT AGT GCC TGA AAG GAG ATA TAA ATG TCT AAA GTA GTG TAT GTG TC
pnn85	GTG ATG ATG CTC GAG TTA GGA TCC TTA CCA TTG CCT ATC GGG AAC ATC
pETiteF	GGA TCC TAA CTC GAG CAT CAT CAC CAC CAT CAC TA
pETiteR	TAT ATC TCC TTC TTA TAG TTA AAC AAA ATT ATT TC

611

612

613

FIGURE LEGENDS

Figure 1: Synthetic pathway for endogenous production of terminal alkenes in *E. coli*

Figure 2: Phylogenetic analysis of $OleT_{JE}$ with the CYP152 P450 enzyme family. $OleT_{JE}$ is shown in the box. The enzymes that have the conserved $OleT_{JE}$ catalytic site residues Phe79, His85, and Arg245 are marked with "*"

Figure 3: (A) Specific and relative specific activities of $OleT_{MC}$ towards linear, saturated C10:0-C18:0 FAs. Each value is an average ± 1 standard deviation ($n \geq 2$). **(B)** Comparison of predicted binding free energies for C10:0-C18:0 FAs between the $OleT_{MC}$ wildtype and mutants. **(C)** Correlation between *in vitro* specific activities and *in silico* binding free energies of $OleT_{MC}$ with various C10:0-C18:0 FAs. **(D)** *In silico* alanine scan of the potential FAs binding pocket with C10:0-C18:0 FAs-$OleT_{MC}$ complexes.

Figure 4: (A) Comparison of the protein structures between the homology model of $OleT_{MC}$ (in yellow) and the crystal structure of C20:0 FA-bound $OleT_{JE}$ (in cyan; PDB:4L40). **(B)** Overlay of the catalytic site structures of $OleT_{MC}$ (in yellow) and $OleT_{JE}$ (in cyan). **(C)** A homology model of $OleT_{MC}$ docked with C18:0 FA. **(D-H)** Overlay of the potential FA binding pocket of the wildtype $OleT_{MC}$ (in yellow) and the $OleT_{MC}$ variants including **(D)** I177W (in red) **(E)** P72M (in blue) **(F)** F296W (in purple) **(G)** I177F (in pink) **(H)** P72F (in gray). Filled red triangles point to the distinctive features in the FA binding pockets of the $OleT_{MC}$ variants as compared to the wildtype.

637 **Figure 5:** Profiles of alkenes production in *E. coli* (**A-C**) EcNN101 and (**E-F**) and EcNN201.

638 (**A, D**) Cell growth and glucose consumption, (**B, E**) Terminal alkene production, and (**C, F**)

639 FA production.

640

641

642 **FIGURE 1**

643

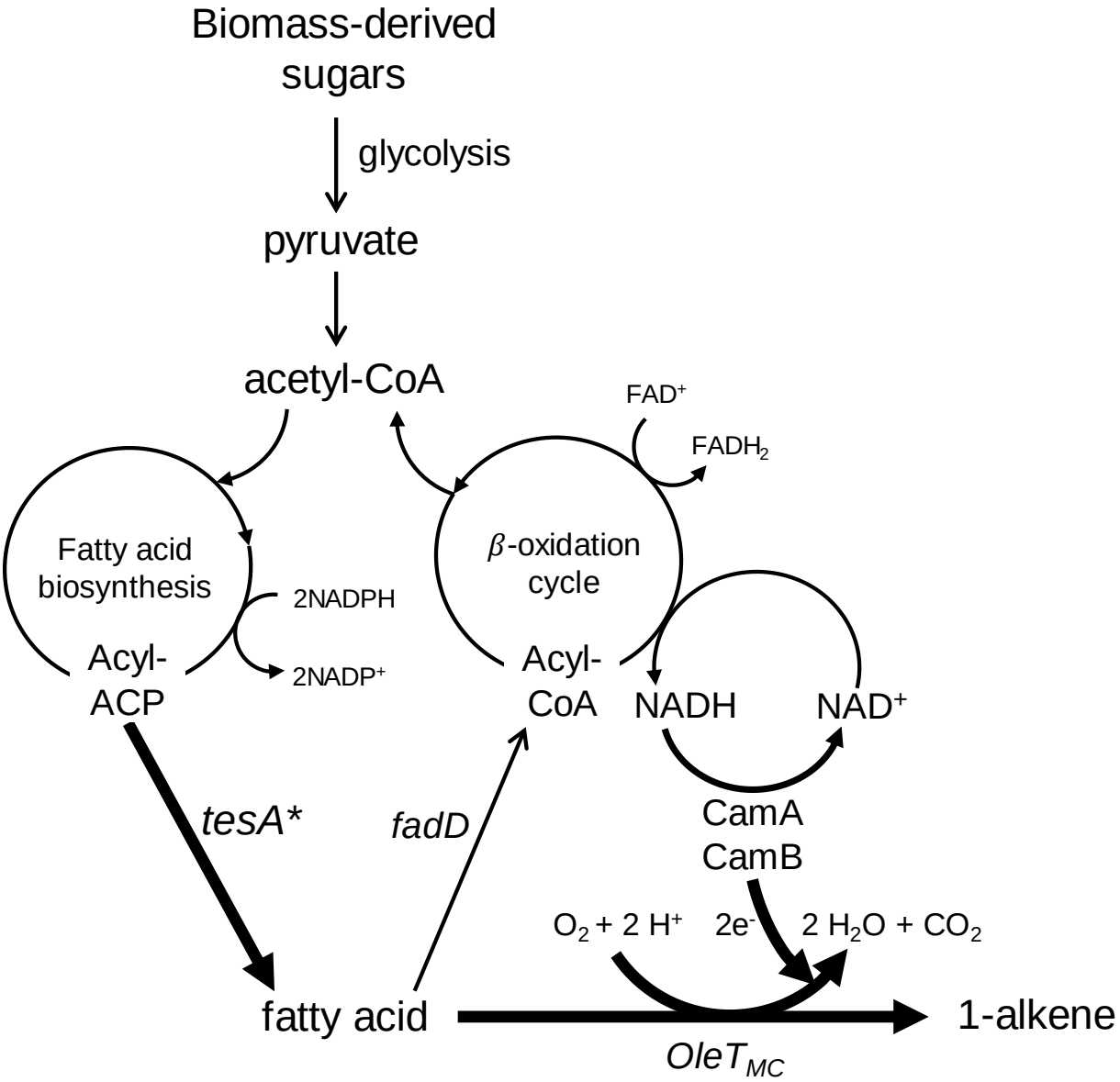

644

645

646 **FIGURE 2**

647

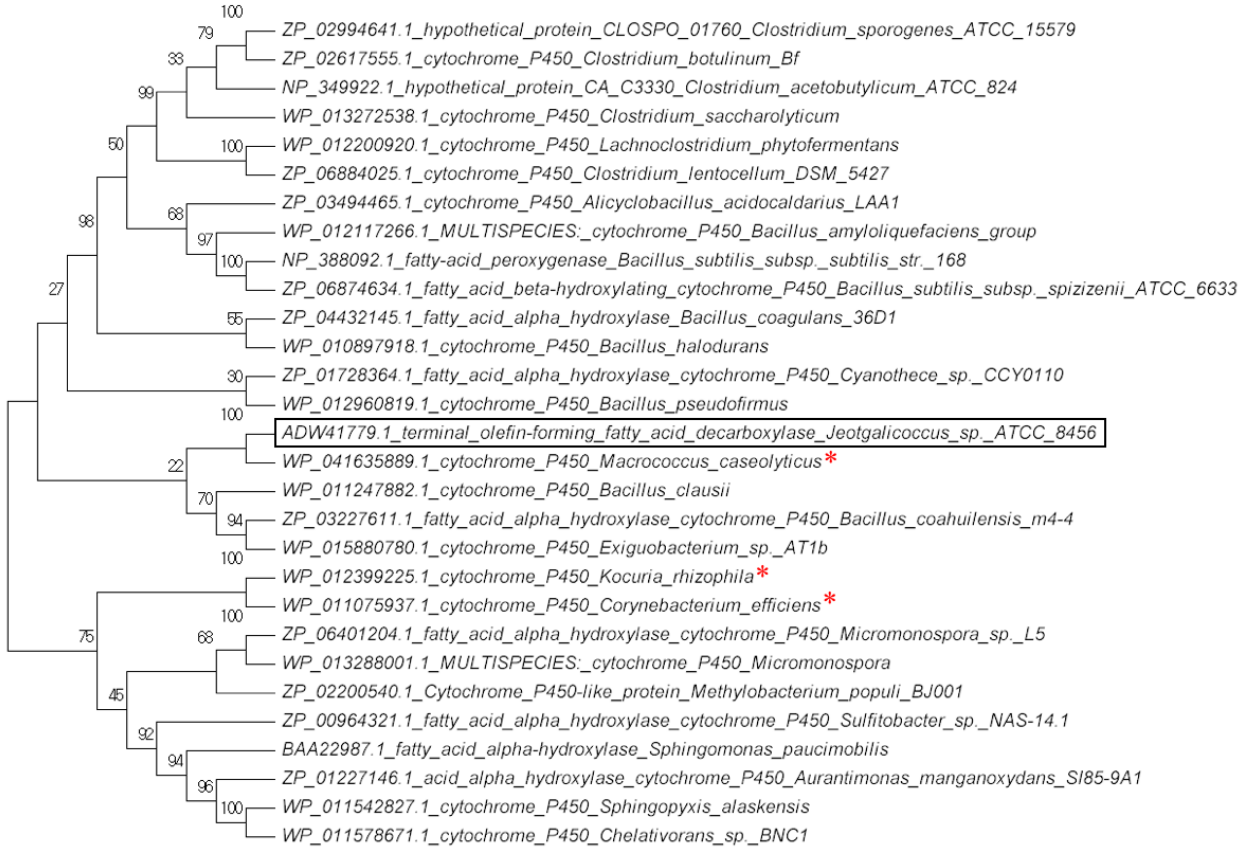

648

649

650 **FIGURE 3**

651

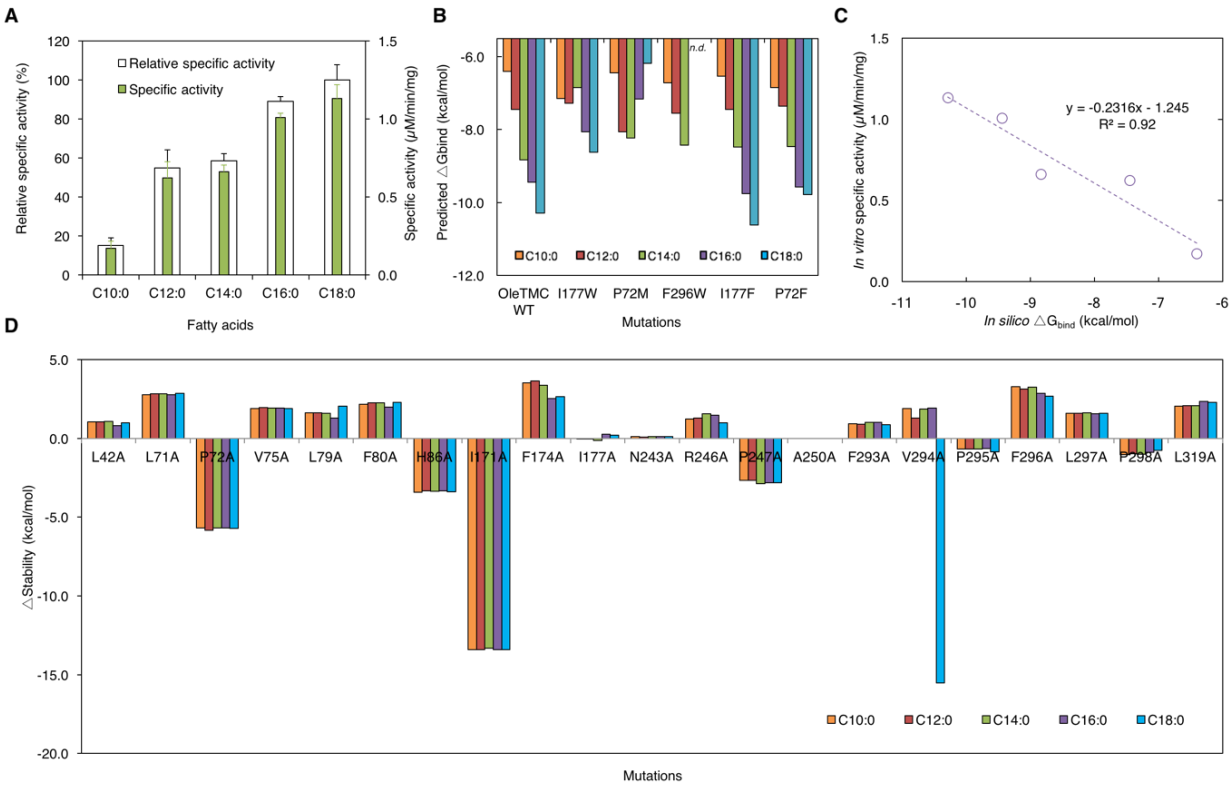

652

653

654 **FIGURE 4**

655

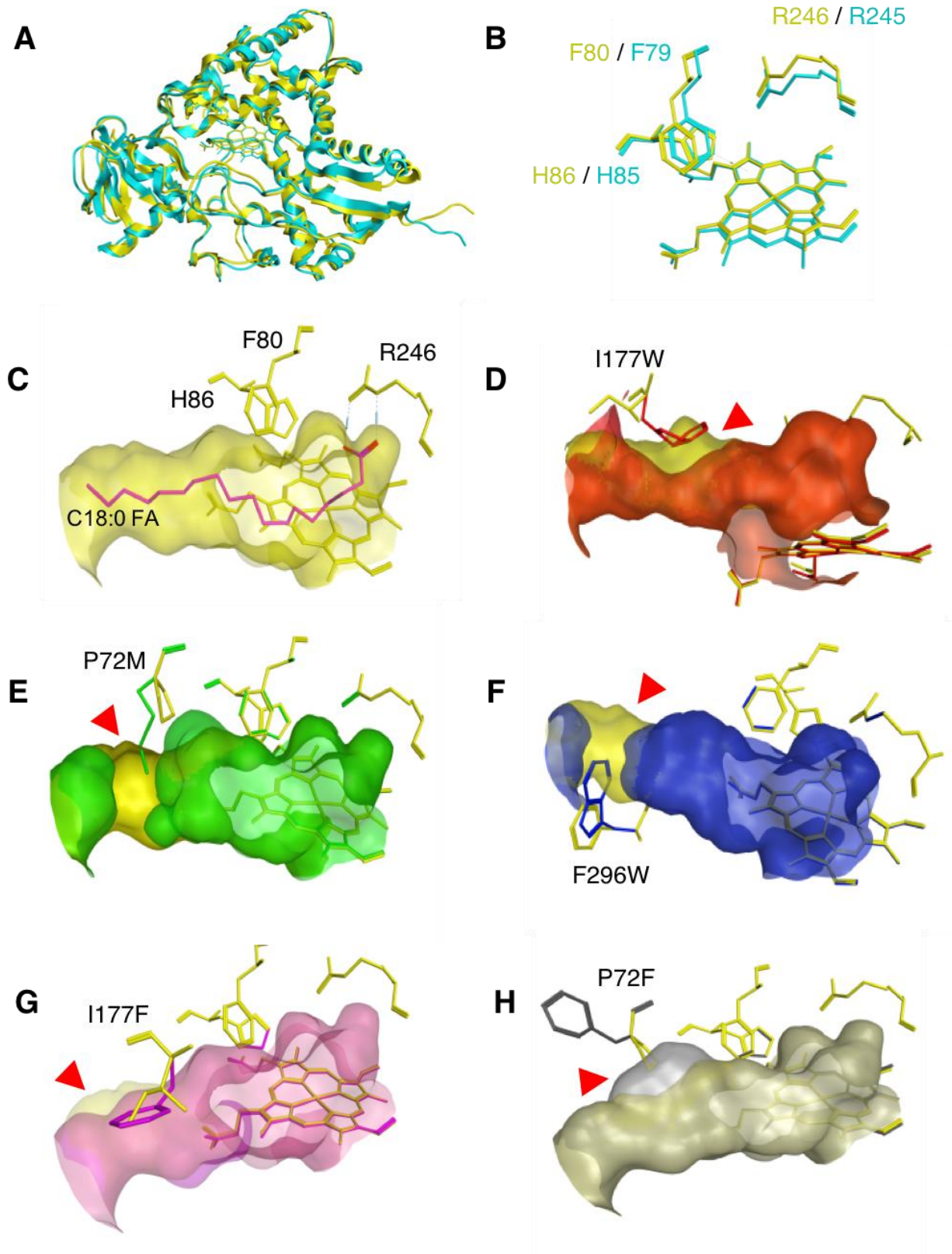

656

657 **FIGURE 5**

658

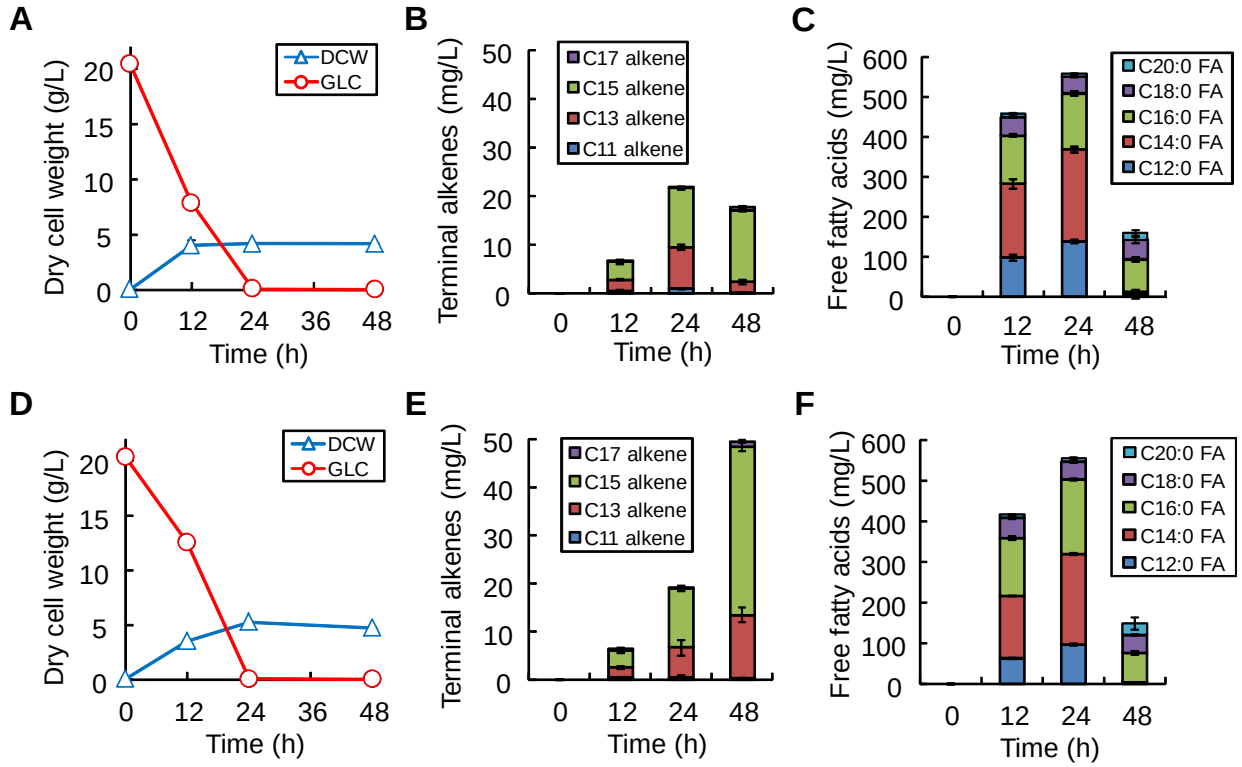

659